JOURNAL OF MATERIALS SCIENCE 30 (1995) 248–252

A high-resolution-electron-microscopy study of a $\gamma/\gamma'-\alpha$ directionally solidified eutectic alloy

Part I *The as-solidified state*

J. Y. DAI, D. X. LI, H. Q. YE, Z. X. JIN, J. H. ZHANG
Laboratory of Atomic Imaging of Solids, Institute of Metal Research, Chinese Academy of Sciences, Shenyang 110015, People's Republic of China

The microstructure of a $\gamma/\gamma'-\alpha$ directionally solidified (DS) eutectic alloy with a nominal composition of Ni–30.26Mo–6.08Al–1.43V (wt %) was investigated by means of high-resolution electron microscopy (HREM) and analytical electron microscopy. The α-fibres exhibited a typical morphology with a rectangular cross-section and they displayed the Bain orientation relationship (OR) with the γ'/γ matrix; that is, $[0\,0\,1]_\alpha \| [0\,0\,1]_{\gamma'}$ and $(1\,1\,0)_\alpha \| (0\,1\,0)_{\gamma'}$. Misfit dislocations and lattice strain fields existed at the α/γ' interface for different habit planes; that is, $(1\,1\,0)_\alpha \| (0\,1\,0)_{\gamma'}$ and $(1\,0\,0)_\alpha \| (1\,1\,0)_{\gamma'}$ were analysed. EDAX (Energy dispersive X-ray) analysis showed that the composition of the γ-phase was approximately $Ni_4(Mo, Al, V)$; it contained 90° rotational domains of $Ni_3(Mo, Al, V)$ with a DO_{22} structure and $Ni_2(Mo, Al, V)$ with a Pt_2Mo structure.

1. Introduction

Nickel-rich directionally solidified (DS) alloys of $\gamma/\gamma'-\alpha$ have received a great deal of interest as candidates for potential high-temperature structural materials. Alloys of this material with eutectic compositions consist of ductile α-Mo fibres and a dual-phase matrix containing a Ni-rich face-centred cubic (f.c.c.) solid solution (γ-phase) and a γ'-Ni_3Al phase with a $L1_2$ structure [1]. These materials have excellent mechanical properties at both high (900–1000 °C) and intermediate (600–850 °C) temperature [2, 3].

The crystallographic orientation relationship and interface structure have been examined because the compatibility in plastic deformation and microstructure thermal stability can be expected to depend on these parameters [4]. Variations in the fibre morphology and in the crystallographic orientation relationships, which depend on the growth rate and on the cooling rate in DS alloys, have been studied systematically [5]. In addition to the Bain orientation relationship, the so-called Pitsch and Nishiyama–Wasserman (NW) orientation relationships between the fibres and the matrix have also been determined. However, a few papers have reported HREM studies of the microstructure in $\gamma/\gamma'-\alpha$ systems.

The purpose of the present work was characterization by means of HREM, of the interface structure of the as-solidified eutectic phases of α and γ', and of the 90° rotational domain structure containing $Ni_3(Mo, Al, V)$ and $Ni_2(Mo, Al, V)$ in the γ-phase.

2. Experimental procedure

The master alloy, with a nominal composition of Ni–30.26Mo–6.08Al–1.43V (wt %), was melted in a vacuum induction furnace to produce 20 cm long rods with diameters of 1.2 cm. Mechanically polished cast bars were directionally solidified in a DS furnace with a growth rate of 1.5 cm h^{-1}. The HREM samples were prepared using a conventional procedure which involved cutting discs with a diameter of 3.0 mm, mechanical polishing them to a thickness of 50 μm, dimpling them to 20 μm and finally ion milling them. The HREM observations were performed in a JEM 2000EX II high-resolution electron microscope with a point-to-point resolution of 0.21 nm. The EDAX analysis was performed in a Phillips EM 420 analytical electron microscope with a probe size of 50 nm.

3. Results and discussion

3.1. The growth morphology and the orientation relationship

Fig. 1 is a typical growth morphology of a DS $\gamma/\gamma'-\alpha$ alloy. α-Mo forms into faceted fibres with rectangular cross-sections which are about one μm in width. The outside regions of the α-Mo, with the bright contrast, are the γ'-Ni_3Al phase; the remaining space is filled by the γ-phase. The α-Mo and the γ'-Ni_3Al are denoted by α and γ', respectively.

Fig. 2 is a composite selected-area electron diffraction (SAED) patterns of γ' and α, in which the weak dots correspond to the superlattice diffraction of γ'-Ni_3Al. It shows that the orientation relationship between the α- and the γ'-phase is $[0\,0\,1]_\alpha \| [0\,0\,1]_{\gamma'}$ and $(1\,1\,0)_\alpha \| (0\,1\,0)_{\gamma'}$. This is a Bain orientation relationship, which is different from the well-known NW and Kurdjumov–Sachs (KS) orientation relationships between the body-centred cubic (b.c.c.) and the f.c.c.

0022–2461

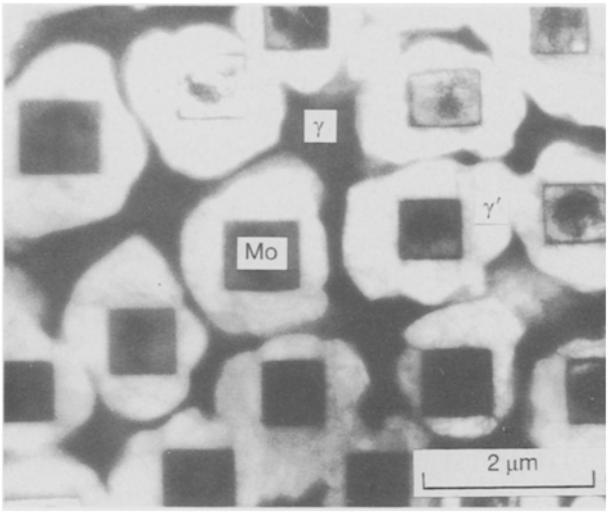

Figure 1 A bright-field electron micrograph along the growth direction of γ/γ′–α DS alloy.

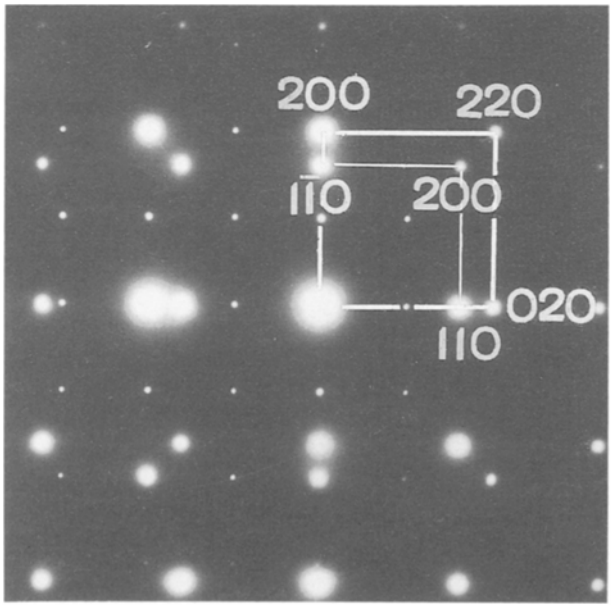

Figure 2 A composite SAED pattern of γ′ and α-Mo.

structures. The orientation relationship between γ′ and γ is $(1\,1\,0)_{\gamma'}\|(1\,1\,0)_{\gamma}$ and $[0\,0\,1]_{\gamma'}\|[0\,0\,1]_{\gamma}$.

3.2. HREM images of the α/γ′ interface viewed along $[0\,0\,1]_{\alpha}\|[0\,0\,1]_{\gamma'}$

Fig. 3a shows a HREM image of $(1\,1\,0)_{\alpha}\|(0\,1\,0)_{\gamma'}$ interface along $[0\,0\,1]_{\alpha}\|[0\,0\,1]_{\gamma'}$. The corresponding electron diffraction pattern is shown in Fig. 2. The average spacing between two atomic positions in the γ′ phase, projected along the $[0\,0\,1]_{\gamma'}$ direction, is 0.18 nm. Therefore, imaging of the atomic positions in the γ′-phase along $[0\,0\,1]_{\gamma'}$ is not possible at the Scherzer focus value, because of the limitation of the point resolution of electron microscope. However, by a suitable selection of the defocus value, the atomic columns in both the α- and the γ′-phase regions are imagined as bright dots.

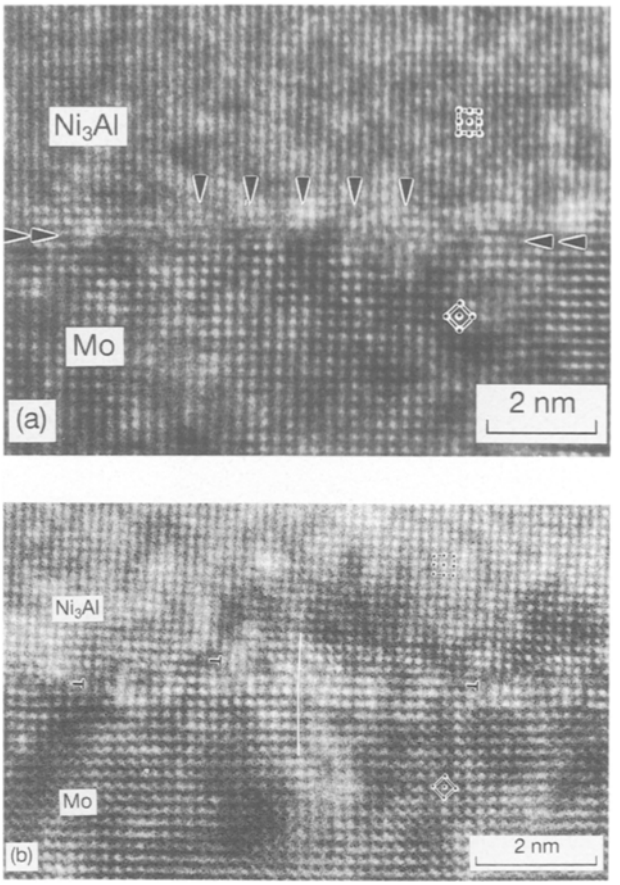

Figure 3 (a) A HREM image of the $(1\,1\,0)_{\alpha}\|(0\,1\,0)_{\gamma'}$ interface viewed along $[0\,0\,1]_{\alpha}\|[0\,0\,1]_{\gamma'}$ and (b) a HREM image of another region showing an array of extra atomic planes, which are indicated by the symbol ⊣, at the interface.

The interface between the α- and γ′-phases, indicated by the double arrows, is atomically flat and without any interfacial phase, as shown in Fig. 3a. The lattice mismatch between $(2\,0\,0)_{\gamma'}$ and $(1\,1\,0)_{\alpha}$ is about $\delta = 21\,\%$. The misfit dislocations, indicated by single arrows, are located at the interface. The Burgers vector of these misfit dislocations is of the type $\boldsymbol{b} = (1/2)\langle 1\,0\,0\rangle_{\gamma'}$, which is parallel to the interface plane. The mean spacing between the dislocations S_d, calculated by $S_d = |\boldsymbol{b}|/\delta$, is 0.9 nm (four atomic planes of $(1\,1\,0)_{\alpha}$), which is in good agreement with the value measured from Fig. 3a. Therefore, the lattice mismatch between the α- and the γ′-phase at the interface appears to be accommodated by the formation of the misfit dislocations.

Fig. 3b shows a HREM image of the α/γ′ interface in the other region of the sample observed along the $[0\,0\,1]_{\alpha}\|[0\,0\,1]_{\gamma'}$ direction. The $(0\,1\,0)_{\gamma'}$ plane is tilted by about 3° with respect to the $(1\,1\,0)_{\alpha}$ plane, which is accommodated by a periodic array of extra atomic planes near the interface indicated by the — symbol.

3.3. HREM image of the α/γ′ interface viewed along $\langle 1\,0\,0\rangle_{\alpha}\|\langle 1\,1\,0\rangle_{\gamma'}$

Fig. 4 is a HREM image of the $(1\,1\,0)_{\alpha}\|(0\,1\,0)_{\gamma'}$ interface, viewed along $[1\,0\,0]_{\alpha}\|[1\,1\,0]_{\gamma'}$. The overlapped image of the α- and the γ′-phase at the 45° inclined interface results in moiré fringes, as shown in the inset

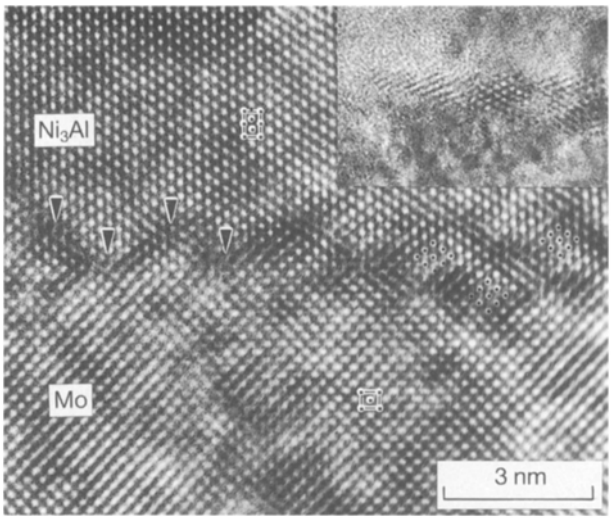

Figure 4. A HREM image of a 45° inclined $(1\,1\,0)_\alpha \| (0\,1\,0)_{\gamma'}$ interface viewed along $[1\,0\,0]_\alpha \| [1\,1\,0]_{\gamma'}$. The inset shows overlapped moiré fringes at the thicker region. At the thinner-edge region, the moiré fringes form a saw tooth-like interface.

of Fig. 4. Because the overlapped region becomes very thin at the edge of the specimen, the interface shows a saw tooth-like shape, as indicated by the arrows. Unfortunately, the study of dislocation structures at this interface becomes difficult using HREM techniques, because the interface dislocations are sheltered by the moiré fringes.

The habit planes of α- fibres are $\{1\,1\,0\}_\alpha$. In a few cases, however, second habit planes corresponding to $\{1\,0\,0\}_\alpha$ and $\{1\,1\,0\}_{\gamma'}$ can also be seen for the same orientation relationship. Fig. 5 is a HREM image of the $(1\,0\,0)_\alpha \| (1\,1\,0)_{\gamma'}$ interface viewed along $[0\,1\,0]_\alpha \| [\bar{1}\,1\,0]_{\gamma'}$. The lattice mismatch between $d^{\alpha}_{(0\,0\,1)}$ and $d^{\gamma'}_{(0\,0\,1)}$ is $\delta = 14\,\%$, and the calculated spacing between the misfit dislocations is 2.5 nm, which is similar to the measured mean distance between the regularly arranged lattice strain fields (as indicated by the arrows in Fig. 5).

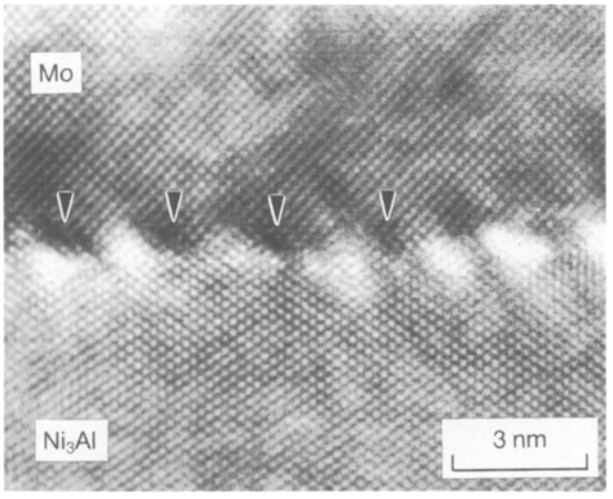

Figure 5 A HREM image of the $(1\,0\,0)_\alpha \| (1\,0\,0)_{\gamma'}$ interface, viewed along $[0\,1\,0]_\alpha \| [\bar{1}\,1\,0]_{\gamma'}$, showing a regular array of the contrast of the lattice strain fields.

3.4. A geometrical description of the $(1\,1\,0)_\alpha \| (0\,1\,0)_{\gamma'}$ and $(1\,0\,0)_\alpha \| (1\,1\,0)_{\gamma'}$ interfaces

In order to understand the interfacial structure of α/γ', the concept of the coincident site lattice (CSL) was employed [6, 7]. Figs 6a and b show a CSL on the $(1\,1\,0)_\alpha \| (0\,1\,0)_{\gamma'}$ and $(1\,0\,0)_\alpha \| (1\,1\,0)_{\gamma'}$ atomic planes, respectively. It has been pointed out by Sriramamurty *et al.* [4] that these two low-energy habit planes should be expected to form in these systems because the similar percentages of coherent atom pairs are about 19% on $(1\,1\,0)_\alpha \| (0\,1\,0)_{\gamma'}$ and 17% on $(1\,0\,0)_\alpha \| (1\,1\,0)_{\gamma'}$, respectively.

The spacing of dislocation lines, projected along $[0\,0\,1)_\alpha \| [0\,0\,1]_{\gamma'}$, in Fig. 6a is four atomic planes of $(1\,1\,0)_\alpha$, which is in good agreement with the experimental observation shown in Fig. 3a. In Fig. 6b, the spacing of the dislocation lines projected along $[0\,1\,0]_\alpha \| [\bar{1}\,1\,0]_{\gamma'}$ would be about 2.5 nm (eight atomic planes of $(0\,0\,1)_\alpha$), which is reasonably close to the mean spacing observed between the lattice strain fields in Fig. 5.

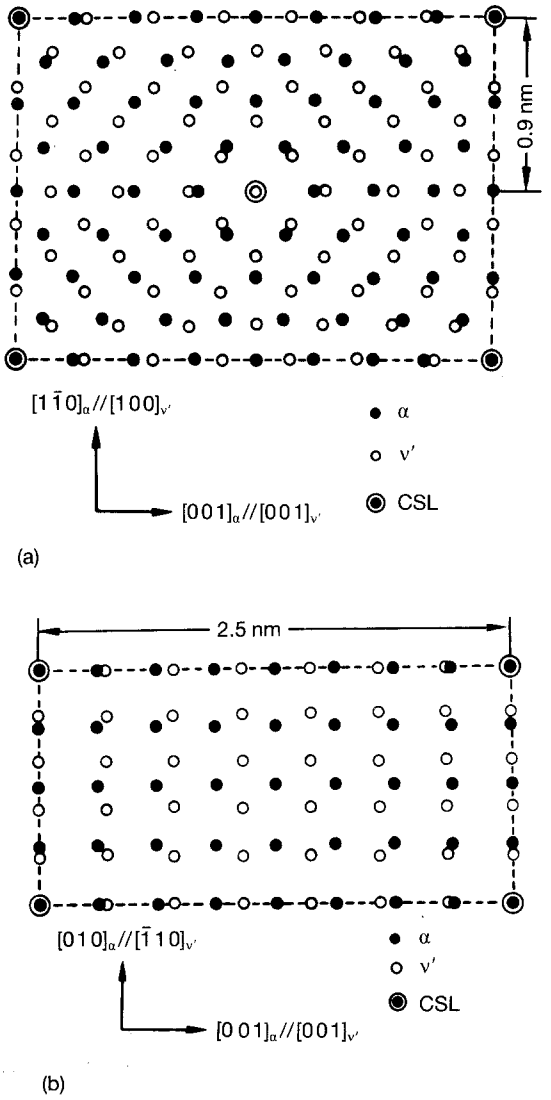

Figure 6 (a) The CSL formed by coinciding planes of $(1\,1\,0)_\alpha$ and $(0\,1\,0)_{\gamma'}$ and (b) the CSL formed by the $(1\,0\,0)_\alpha \| (1\,1\,0)_{\gamma'}$ habit planes. Only one layer of each lattice is included.

3.5. The domain structure and the domain boundary in the γ-phase

The results of EDAX analysis in the γ-phase showed that the γ-phase contains about 81 at % Ni, 12 at % Mo, 4 at % Al and 3 at % V, which can be denoted approximately by $Ni_4(Mo, Al, V)$. Figs 7a and b are the SAED pattern and schematic diagram of the indexed pattern, showing the presence of 90° rotational domains of $Ni_3(Mo, Al, V)$ and $Ni_2(Mo, Al, V)$ with DO_{22} and Pt_2Mo type structures, respectively. Fig. 7c is a doubly exposed dark-field image using the diffraction spots marked as 1 and 2 in Fig. 7b, showing the lens-shaped $Ni_2(Mo, Al, V)$ precipitates in the γ-matrix. The domain size of the $Ni_2(Mo, Al, V)$ phase ranges from tens of nanometres to one or two hundreds of nanometres.

The crystal structure of the Ni_xMo phases, where $x = 2$, 3 and 4, can be described as a regular arrangement of Ni or Mo atomic planes on the {4 2 0} planes of the f.c.c. parent [8]. The Ni_2Mo, Ni_3Mo and Ni_4Mo have two, three and four layers of Ni planes between adjacent Mo planes, respectively.

Fig. 8a is a HREM image of a triple interface between $Ni_2(Mo, Al, V)$ and the 90° rotational domains of $Ni_3(Mo, Al, V)$ viewed along the ⟨0 0 1⟩ direction of $Ni_3(Mo, Al, V)$ and $Ni_2(Mo, Al, V)$. The interfaces are parallel to the {1 1 0} planes of $Ni_2(Mo, Al, V)$ and $Ni_3(Mo, Al, V)$. The 90° rotational domain boundary in $Ni_3(Mo, Al, V)$ is indicated by the arrows in Fig. 8a. The unit cells of $Ni_2(Mo, Al, V)$ and $Ni_3(Mo, Al, V)$ are also outlined in the HREM image.

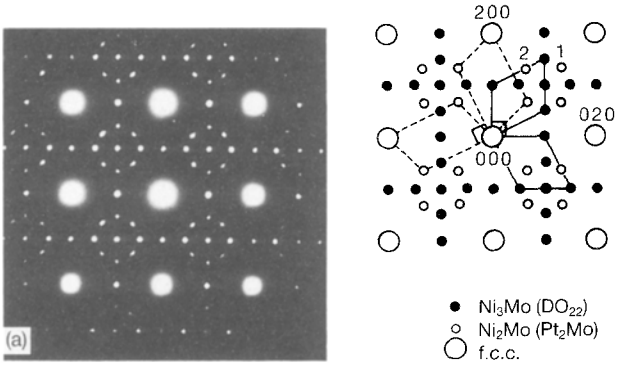

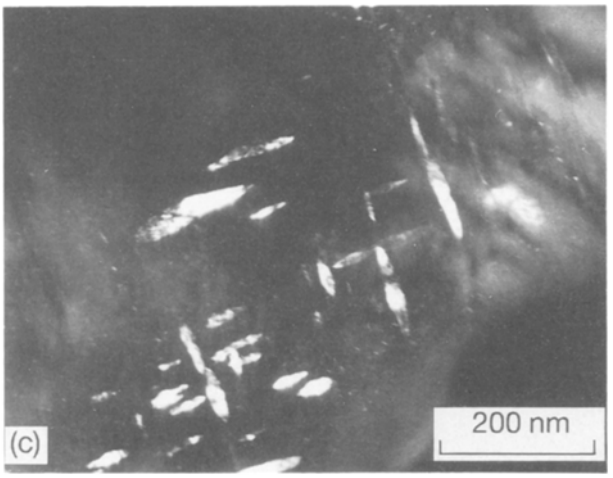

Figure 7 (a) The electron diffraction pattern for the γ-phase along the ⟨0 0 1⟩ zone axis, (b) a schematic diagram of 90° rotational domains of $Ni_2(Mo, Al, V)$ with a Pt_2Mo-type structure and DO_{22} form $Ni_3(Mo, Al, V)$, and (c) a doubly exposed dark-field micrograph of $Ni_2(Mo, Al, V)$ precipitates using the superlattice spots marked as 1 and 2 in (b).

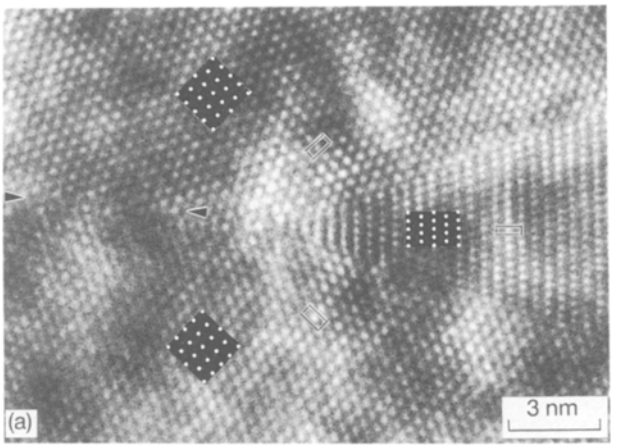

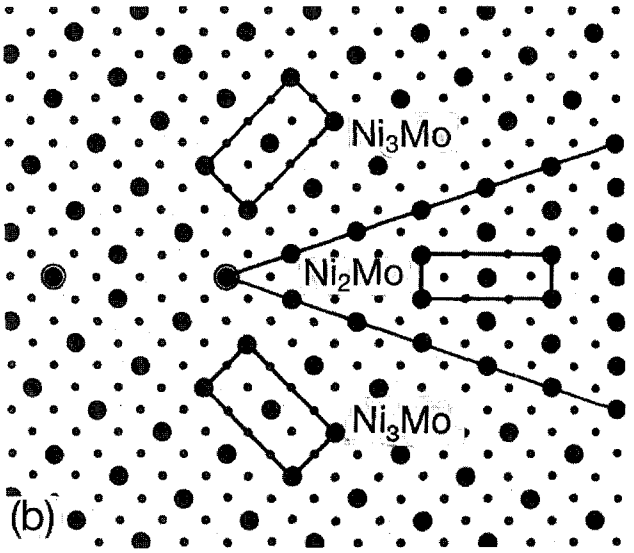

Figure 8 (a) A HREM image of lens-shaped $Ni_2(Mo, Al, V)$ precipitated inside two 90° rotational domains of $Ni_3(Mo, Al, V)$. The interfaces between $Ni_2(Mo, Al, V)$ and $Ni_3(Mo, Al, V)$ are parallel to the {1 1 0} planes. The 90° rotational domain boundary is indicated by the arrows, (b) The structural model of the Ni_2Mo/Ni_3Mo interface projected along the ⟨0 0 1⟩ directions. (●) Mo atoms and (•) Ni atoms.

In order to analyse the structural model of the interface, image simulations were performed for $Ni_2(Mo_{0.6}, Al_{0.2}, V_{0.2})$ and $Ni_3(Mo_{0.6}, Al_{0.2}, V_{0.2})$ using the operating parameters of JEM 2000EX II; that is, the coefficient of spherical aberration $C_s = 0.7$ mm, the semiangle of the beam divergence $\alpha = 0.75$ mrad and the half width of the Gaussian defocus spread $\triangle = 8$ nm. The insets in Fig. 8a are simulated images for a thickness of 12.5 nm and a defocus value of 55 nm. Each bright dot in the image of the $Ni_2(Mo_{0.6}, Al_{0.2}, V_{0.2})$ and the $Ni_3(Mo_{0.6}, Al_{0.2}, V_{0.2})$ regions corresponds to the position of a $(Mo_{0.6}, Al_{0.2}, V_{0.2})$ atomic column.

Fig. 8b is a projected structural model of the interface between Ni_2Mo and Ni_3Mo, which is shown in Fig. 8a. The interface is parallel to the {1 1 0} planes of Ni_3Mo and Ni_2Mo, and the Mo atomic plane is the common plane at the interface.

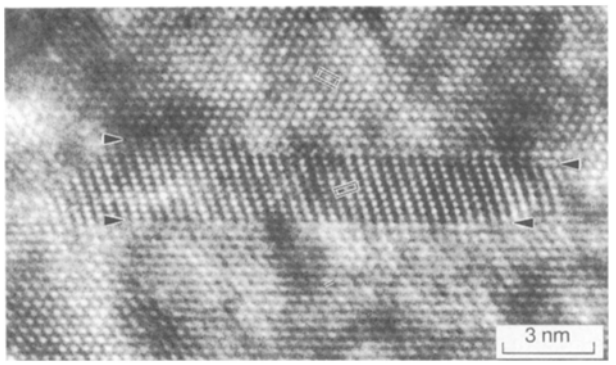

Figure 9 A HREM image of a $Ni_2(Mo, Al, V)$ plate which has precipitated in an $Ni_3(Mo, Al, V)$ matrix.

Occasionally, a fine $Ni_2(Mo, Al, V)$ plate can also precipitate in the $Ni_3(Mo, Al, V)$ matrix. Fig. 9 is a HREM image of a $Ni_2(Mo, Al, V)$ plate precipitated in a $Ni_3(Mo, Al, V)$ matrix. The interface is also parallel to $\{1\,1\,0\}$ planes of $Ni_3(Mo, Al, V)$ and $Ni_2(Mo, Al, V)$. Ledges with a height equal to one or two layers of the (Mo, Al, V) atomic planes can sometimes be found at the interface.

4. Conclusions

1. A majority of α-fibres exhibit a typical morphology with rectangular cross-sections, and they display the Bain orientation relationship with the γ'/γ matrix; that is,

$[0\,0\,1]_\alpha \| [0\,0\,1]_{\gamma'}$ to the growth direction

$(1\,1\,0)_\alpha \| (0\,1\,0)_{\gamma'}$ to the habit plane

The $\{1\,1\,0\}_\alpha$ facets are also observed in a few cases for the same orientation relationship.

2. HREM images of the $(1\,1\,0)_\alpha \| (0\,1\,0)_{\gamma'}$ interface along the growth direction show an array of misfit dislocations at the interface, which accommodate the 21 % lattice mismatch between $d^{\alpha}_{(1\,1\,0)}$ and $d^{\gamma'}_{(2\,0\,0)}$.

3. Besides the misfit dislocations, lattice strain fields with a spacing of about 2.5 nm were observed near the $(1\,0\,0)_\alpha \| (1\,1\,0)_{\gamma'}$ interface.

4. EDAX analysis showed that the composition of the γ-phase is approximately $Ni_4(Mo, Al, V)$, which contained 90° rotational domains of $Ni_3(Mo, Al, V)$ (with a DO_{22} structure) and $Ni_2(Mo, Al, V)$ (with a Pt_2Mo structure).

Acknowledgements

This project was supported by the National Nature Science Foundation of China (NSFC) and the National Advanced Materials Committee of China (NAMCC) on Grant No. 59291000, and by the Committee of Science and Technology of Liaoning Province on Grant No. 92001 (J. Y. Dai)

References

1. H. SPRENGER, H. RICHTER and J. J. NICKL, *J. Mater. Sci.* **11** (1976) 2075.
2. D. D. PEARSON, B. H. KEAR and F. D. LEMKEY, in International Conference on Creep and the Fracture of Engineering Materials and Structures, University College, Swansea, 1981, edited by B. Wilshire and D. R. J. Owen (Pine Ridge Press, 1981) p. 213.
3. R. E. ANDERSEN, A. R. COX, T. D. TILLMAN and E. C. VAN REUTH, in Proceedings of the 2nd International Conference on Rapid Solidification Processing, Baton Rouge, LA, 1980, edited by R. Mehrabian, B. H. Kear and M. Cohen (Claitor's Publishing Division, 1980) p. 416.
4. A. M. SRIRAMAMURTY, D. BANERJEE and S. N. TEWARI, *Acta Metall.* **30** (1982) 1231.
5. E. BLANK, P. HENRIQUEZ and W. FUNK, *ibid.* **37** (1989) 229.
6. W. BOLLMANN, "*Crystal defects and crystalline interfaces*" (Springer, Berlin, 1970).
7. R. W. BALLUFFI, A. BROKMAN and A. H. KING, *Acta Metall.* **30** (1982) 1453.
8. P. R. OKAMOTO and G. THOMAS, *ibid.* **19** (1971) 825.

Received 11 August 1993
and accepted 16 May 1994